



Ultra-compact, efficient and high-polarization-extinction-ratio polarization beam splitters based on photonic anisotropic metamaterials

JINGJING ZHANG,¹ XIAODONG SHI,²  ZHAOJIAN ZHANG,³  KAI GUO,^{4,5}  AND JUNBO YANG^{3,6}

¹*Institute of Mirco/Nano Optoelectronic and Terahertz Technology, Jiang Su University, Jiangsu 210010, China*

²*DTU Fotonik, Technical University of Denmark, DK-2800 Lyngby, Denmark*

³*Department of Physics, National University of Defense Technology, Changsha 410073, China*

⁴*Institute of Systems Engineering, AMS Beijing, Beijing 100141, China*

⁵*guokai07203@hotmail.com*

⁶*yangjunbo@nudt.edu.cn*

Abstract: Anisotropic metamaterials (AM) provide a new avenue for a next-generation silicon platform to design ultra-compact, densely integrated optical components, thus functional devices based on AM are drawing increasing attention recently. Here, we propose a novel efficient polarization beam splitter (PBS) with high polarization extinction ratio based on AM. An ultra-compact coupling region of $2.5 \times 14 \mu\text{m}^2$ is achieved by tailoring the AM structures, which can efficiently suppress the TE mode coupling, and enhance the TM mode coupling in the directional couplers simultaneously. The insertion loss is simulated to be as low as <0.2 dB within a bandwidth of 70 nm for both modes, and the polarization extinction ratio is as high as 46 dB and 33 dB for TE and TM modes, respectively. We also experimentally demonstrate the proposed PBS, with low insertion loss of 1 dB, high extinction ratio of >20 dB and wide operational bandwidth of >80 nm.

© 2021 Optica Publishing Group under the terms of the [Optica Open Access Publishing Agreement](#)

1. Introduction

Integrated photonic circuits (PIC) are widely used for optical communication, metrology, spectroscopy, quantum computing and communication, thanks to the superior advantages of small device size, low power consumption, and compatibility with the complementary metal-oxide-semiconductor (CMOS) technology [1,2]. Due to the high refractive index contrast between silicon and the cladding materials, the silicon-on-insulator (SOI) platforms offer compact and efficient photonic devices than other integrated platforms such as InP, LiNbO₃, SiC, and SiN [3–7]. Large-scale on-chip systems with compact and small devices show a high promise in recent years. Especially, on-chip quantum computing systems have been demonstrated to realize quantum walk, qubit exchange and high dimensional quantum entanglement, and more than 200 photonic devices have been integrated in a small single chip [8–11].

Polarization beam splitter (PBS), as an important device in PIC for multiplexing and demultiplexing polarizations, is widely used in polarization handling systems and polarization encoding communication systems [12–14]. The research of PBS usually considers four aspects, including efficiency, polarization extinction ratio, wavelength bandwidth, and footprint. Various types of PBS have been demonstrated, such as directional couplers (DC) [15–17], multimode interference (MMI) [18–20], and asymmetrical directional couplers (ADC) [15,21], and plasmonic waveguides [22,23]. However, these structures usually suffer from large footprint, narrow bandwidth, low fabrication tolerance, or low polarization extinction ratio. The DC-based PBS usually suffers

from large footprint and low polarization extinction ratio [15]. The MZI-based PBS shows high efficiency and large polarization extinction ratio. However, the large device size of $> 100 \mu\text{m}$ brings challenges for compact PIC systems. The ADC-based PBS can achieve high polarization extinction ratio of 20 dB, but the narrow operating wavelength bandwidth limits the applications that require wide bandwidth. Although the inverse design transformation or machine learning are able to realize ultra-compact PBS, complex fabrication processes make them difficult to be compatible with other devices, and phase variability can cause extra scattering loss [24–27]. It is possible to add a periodic subwavelength structure, such as photonic crystals, which can form a forbidden band to filter out one of the polarizations and improve the polarization extinction ratio, but it will also introduce extra scattering loss [28].

Anisotropic metamaterials (AM) is a technology, that breaks through the limitation of some apparent natural laws by the periodic and ordered structure design of physical dimensions of materials, and obtains the abnormal functions and effects beyond the original physical characteristics of nature [29]. Using metamaterials, invisible cloaking [30,31], flattened lens [32,33], anomalous refraction [34] and reconfigurable all-dielectric metalens [35] have been achieved in the silicon platforms. AM structures have also been used to design the PBS, with low insertion loss, broad bandwidth and high polarization extinction ratio [36–39]. Using the anisotropic properties of subwavelength gratings metamaterials to design the PBS shows wide working bandwidth of $> 100 \mu\text{m}$ and low insertion loss of $< 1 \text{ dB}$, but it suffers from large footprint [36]. The length of the PBS using the subwavelength grating AM can be reduced to $< 20 \mu\text{m}$ by using SU8 as the cladding material, but most of the SOI photonic circuits use air or silica as the cladding materials, which makes this device incompatible with the normal photonic circuits in polarization controlling systems [37]. It is known that the all-dielectric metamaterials are able to make anisotropic crystal structures, making possible large refractive index contrast between two orthogonal modes propagating in the waveguides [29]. Thus, with this property, it is still worthy to explore the PBS utilizing AM to exhibit peculiar optical effects and advantages, including low loss, high polarization extinction ratio, wide bandwidth, and ultra-compact size.

In this paper, we propose an ultra-compact subwavelength-strips-based AM polarization beam splitter with low insertion loss and ultra-high polarization extinction ratio. The analysis of the coupled mode theory shows that the effective refractive indices of the asymmetric and symmetric modes are almost equivalent for the TE polarization, but show large difference for the TM polarization, with the proposed AM. Therefore, the structures are able to strongly suppress the coupling for the TE polarization, and enhance the coupling for the TM polarization, simultaneously, within a short coupling length. The simulated polarization extinction ratio is

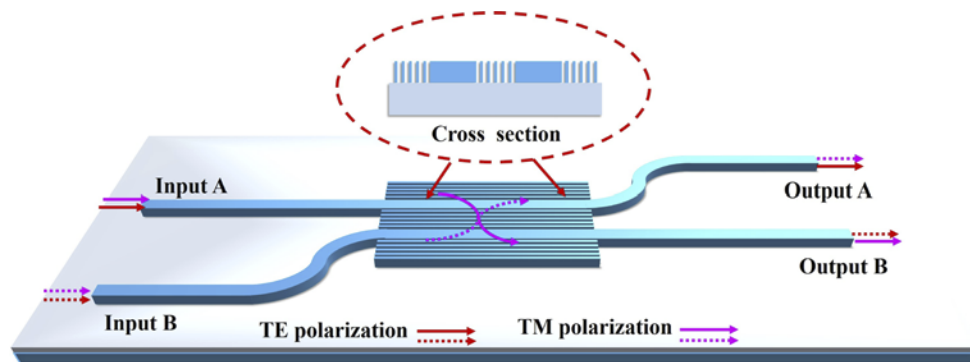


Fig. 1. The 3D schematic view of the AM PBS.

higher than 40 dB and 30 dB for the TE and TM polarizations within a small area of $2.5 \times 14 \mu\text{m}^2$, respectively.

The device, shown in Fig. 1, is designed on the SOI platform with a 220-nm Si top layer and a $2 \mu\text{m}$ SiO_2 buffer layer. The width of the two single-mode waveguides is 500 nm. We define the input of the directional couplers as Input A and Input B, and the output of directional couplers as Output A and Output B. The coupling region of the PBS is composed of two parallel waveguides with AM, which is composed of identical periodic subwavelength strips. When light beam is launched into Input A or Input B, the TE polarized light remains in the same waveguide, while the TM polarized light is coupled to the other waveguide.

2. Principle and design

We use the coupling theory of the directional coupler to design the AM PBS. The length of the PBS is determined by [40]

$$L_c = \frac{\lambda}{2(n_{\text{odd}} - n_{\text{even}})}, \quad (1)$$

where λ , n_{even} and n_{odd} are the incident wavelength, effective refractive indices of even symmetric and odd symmetric modes, respectively. The electric field distribution without and with AM for odd and even modes are shown in Fig. 2, simulated in COMSOL Multiphysics Software. The AM here is composed of periodic strips with period of $T = 100$ nm, filling factor of $f = 0.5$, and the number of cycles of $N = 5$, on both sides of the single-mode waveguides. As can be seen, with the proposed AM structure, the effective refractive index of the TM mode can be largely changed than that of the TE mode.

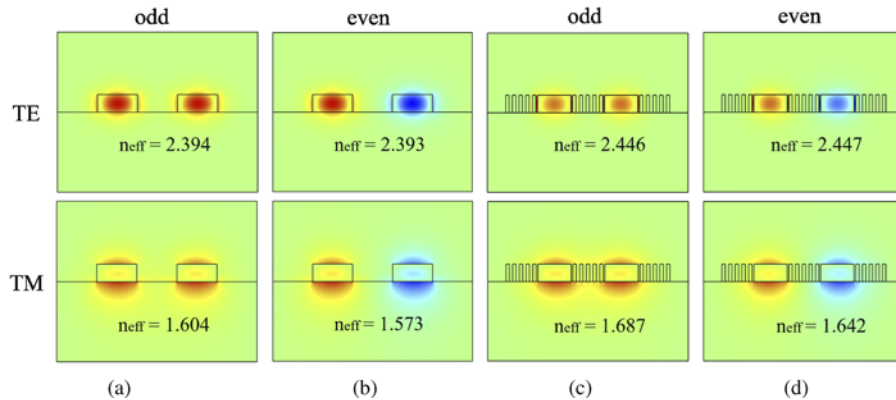


Fig. 2. The electric field distribution of TE and TM modes in the coupling waveguides with and without AM structures.

Then, we analyze the effective refractive indices of odd and even modes for TE and TM polarizations with and without AM as a function of the waveguide gap, shown in Fig. 3(a) and 3(b), respectively. In the simulation, the gap is changed with a step of 100 nm, and the period and the filling factor are fixed as 100 nm and 0.5. The number of cycle is determined by the gap. With AM structures, the effective refractive index difference of the TE polarization between the odd and the even modes slightly decreases with the increasing gap, while that of the TM polarization increases generally. As a result, the coupling length of the TE and TM polarizations has much larger difference, according to Eq. (1).

Next, we use Lumerical FDTD Solutions for the rest simulation. We plot the coupling length of the PBS versus the gap with and without AM in Fig. 3(c) and Fig. 3(d). As can be seen, the coupling length of the PBS increases with the increasing gap for both polarizations. Thus, the

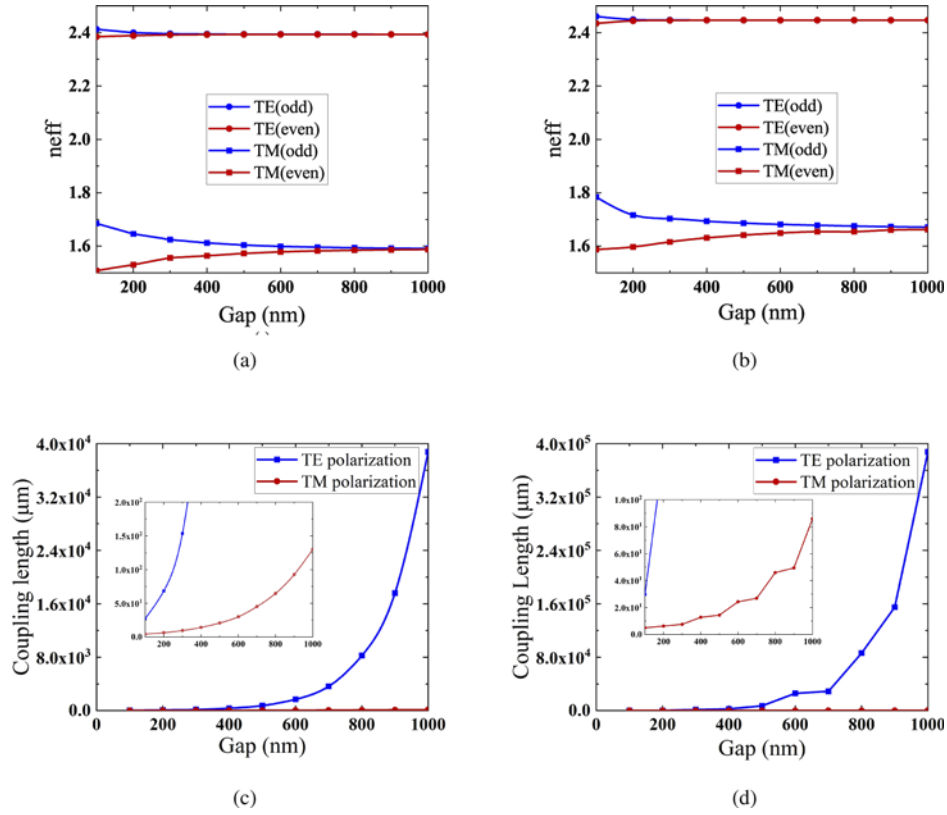


Fig. 3. The effective refractive index versus the gap for (a) normal PBS and (b) AM PBS. The coupling length versus the gap for (c) normal PBS and (d) AM PBS.

coupling length of the TM polarization is significantly shorter than that of TE polarization. It means that within a short coupling length, the TM polarization can be largely coupled to the other waveguide, while the TE polarization is minimally coupled, which enables effectively polarization beam splitting. When the gap is < 300 nm, the AM has less effect on the coupling length for both polarizations. When the gap is > 300 nm, the coupling length of the TE polarization becomes much longer in the AM PBS than that in the normal PBS. On the other hand, the coupling length of the TM polarization becomes shorter in the AM PBS than that in the normal PBS. We choose the typical gap of 500 nm, and calculate the coupling length for the TE and TM polarizations to be $7110 \mu m$ and $14.6 \mu m$, respectively. According to the coupled mode theory, the power distribution along the two coupled waveguides are expressed as

$$P_A = \cos^2 \frac{\pi}{2L_c} L \quad (2)$$

$$P_B = \sin^2 \frac{\pi}{2L_c} L \quad (3)$$

where P_A and P_B are the power distribution in the two waveguides, and L is the length of the waveguides. When $L = L_c$, the light coupling from Input A will completely be coupled into Output B theoretically. We calculate the polarization extinction ratio (PER) of the PBS with and without the AM structure for TE and TM polarizations is defined as

$$PER_{TE} = -10 \log \frac{P_{PortA,TE}}{P_{PortB,TE}}, \quad (4)$$

and

$$PER_{TM} = -10 \log \frac{P_{PortB, TM}}{P_{PortA, TM}}. \quad (5)$$

The simulated PER of 63 dB and 85 dB be achieved for the TE polarization in the normal PBS and AM PBS, respectively, while the PER for the TM polarization is infinite. Such strong suppression of the TE polarized light is because the electric field of the TE mode is oscillated along the horizontal direction. According to the Maxwell–Garnett effective medium theory (EMT), when the multilayer subwavelength period is $T \ll \lambda$, the device shows strong anisotropy at the operating wavelength for TE polarization [40]. The permittivity along the vertical and horizontal direction follows

$$\varepsilon_V = f\varepsilon_{Si} + (1-f)\varepsilon_{air} \quad (6)$$

and

$$\varepsilon_H = \frac{\varepsilon_{Si}\varepsilon_{air}}{f\varepsilon_{Si} + (1-f)\varepsilon_{air}} \quad (7)$$

where ε_{Si} and ε_{air} are the permittivities of Si and air, respectively. The skin depth is reduced by the AM structure for the TE polarization. On the other hand, the electric field of the TM mode oscillates along the vertical direction, which will not be affected by the suppression of the evanescent light coupling. The subwavelength structure, filling into the PBS, can induce an increase of the TM mode refractive index, as shown in Fig. 3(b). Therefore, by adding the periodic subwavelength strips, one can effectively suppress the TE mode coupling and efficiently enhance the TM mode coupling within a short coupling length, realizing polarization beam splitting with high polarization extinction ratio. Therefore, the calculated AM parameters of the proposed PBS are summarized as following: $T=100$ nm, $f=0.5$, $N=5$ and $L_c=14.6$ μm , which are used as the starting reference of the following optimization.

We simulate the performance of PBS through the 3D finite-difference time domain (FDTD) for further optimization, by sweeping the coupling length, the width of the subwavelength strips, and the period [41]. Transmission for the optimized structure is shown in Fig. 4.

The transmission as a function of the coupling length is shown in Fig. 4, from 13 to 17 μm . The transmission efficiency of the PBS is $> 99\%$ and 94% for TE and TM polarization, respectively. The PER is extracted from Fig. 4, which is > 20 dB and insertion loss is < 0.2 dB for both polarizations from 13 μm to 14.8 μm . Especially at the coupling length of 14.0 μm , high polarization extinction ratio of 46 dB and 32 dB can be realized for TE and TM polarizations, respectively. The strip width, related to the filling factor, of the AM structure, can influence the effective refractive index of the modes with different polarizations. Thus, we sweep the width from 20 to 70 nm, seen in Fig. 4(b). The PBS exhibits high transmission efficiency of $> 99\%$ and 92% for TE and TM polarizations, respectively. The PER is > 20 dB and insertion loss is < 0.2 dB for both polarizations from 30 nm to 60 nm. With the width of 50 nm, the PER is 46 dB and 32 dB for TE and TM polarizations, respectively. Finally, we choose the coupling length of $L=14$ μm , the strip width of $w=50$ nm, as the optimized structural parameters to analyze the period of subwavelength periods in the coupling region, shown in Fig. 4(c). In the periodic range from 80 nm to 120 nm, the PBS shows high transmission of $> 99\%$ and 94% for TE and TM polarizations, respectively, with a high polarization extinction ratio of more than 20 dB for both polarizations. Considering the fabrication tolerance, we choose the coupling length of 14 μm , the width of 60 nm, and the period of 120 nm, as the optimized parameters for the AM PBS, so that the number of cycle is 4. Using these parameters, we simulate the transmission efficiency and PER as a function of the wavelength from 1.45 to 1.65 μm , shown in Fig. 4(d) and 4(e). The PBS exhibits high transmission efficiency of $> 80\%$ for both polarizations, respectively, corresponding to an insertion loss of 1 dB, in a broad bandwidth between 1470 nm and 1570 nm. The PER is more than 20 dB for both polarizations from 1520 nm to 1550 nm. Especially, the PER is > 35 dB for the TE polarization within the 200 nm bandwidth.

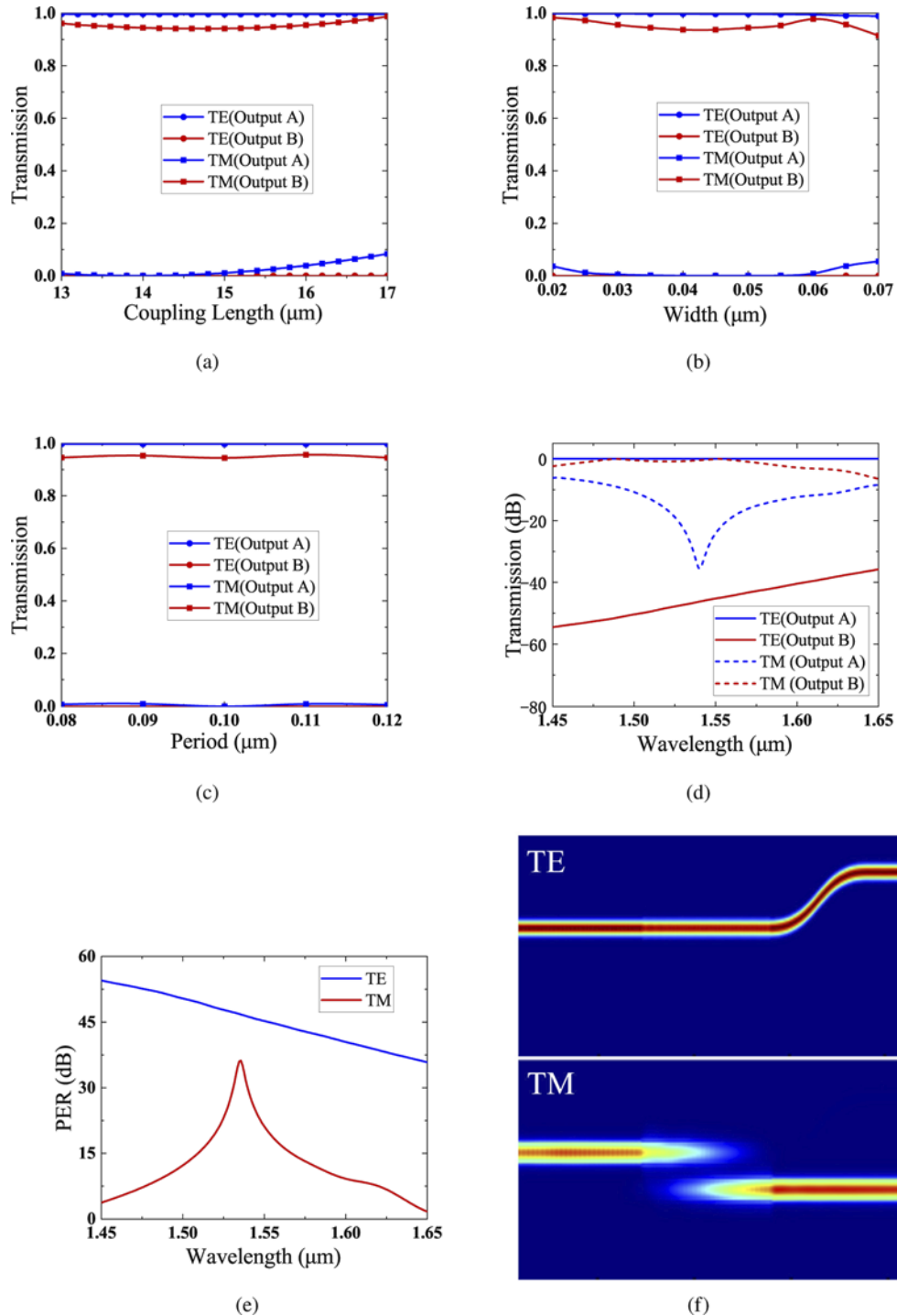


Fig. 4. The transmission versus (a) coupling length, (b) strip width, (c) period of the AM PBS. (d) The transmission and (e) the PER versus wavelength. (f) The optical energy distribution of the optimized AM PBS.

With these optimized parameters, we simulate the optical energy distribution of TE and TM polarized light along the AM PBS, shown in Fig. 4(f). When the light is launched from Input A, the TE polarized light transmits directly to Output A, and TM polarized light is coupled to Output B. The results indicate that the proposed AM PBS works effectively.

The optimized parameters of the proposed AM-based PBS, are listed in Table 1. Here, L_c , g , w , f , λ and N are the coupling length, gap, single-mode waveguide width, filling factor, period, and the number of cycle.

Table 1. The optimized parameters of PBS.

PBS	$L_c = 14 \mu\text{m}$	$g = 500 \text{ nm}$	$w = 500 \text{ nm}$
AM	$f = 0.5$	$\lambda = 0.12 \mu\text{m}$	$N = 4$

3. Fabrication and measurement

Using the optimized parameters, we fabricate the device. The device fabrication starts from a SOI chip, with a 220 nm top silicon thin film and a 2 μm buried oxide layer. The pattern is defined on the e-beam resist by e-beam lithography, and is then transferred to the silicon thin film by the ICP-RIE dry etching. Fig. 5 shows the scanning electron microscope images of the fabricated PBS. Identical grating couplers are connected to the four ports of PBS for testing the device.

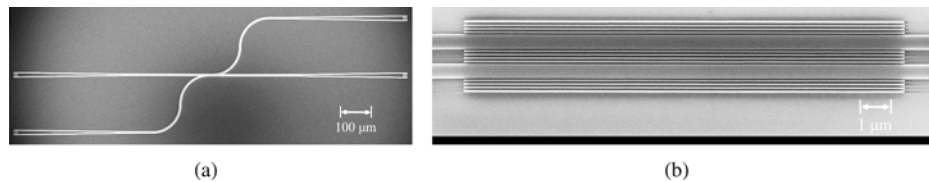


Fig. 5. (a) SEM image of the testing device. (b) Zoom-in SEM image of the AM PBS in the center of the testing device.

We build the measurement setup, shown in Fig. 6, for characterization. A tunable CW laser source launches light into a polarization controller, to adjust the polarizations. The polarized light is coupled in and out of the device between the device and the fiber. An optical spectrum analyzer is used to measure the transmission spectrum.

The normalized transmission efficiency in the AM PBS of the TE and TM polarized light between 1520 nm and 1620 nm is plotted in Fig. 6(b) and 6(d) with input light from Input A and Input B. The maximum transmission efficiency of TE and TM polarized light is more than 80%, equivalent to an insertion loss of <1 dB. The transmission efficiency generally decreases with increasing wavelength. The polarization extinction ratio versus the wavelength is plotted in Fig. 6(d) and Fig. 6(e). As can be seen, the polarization extinction ratio is >20 dB from 1520 nm to 1595 nm for both TE and TM polarizations. Especially, the polarization extinction ratio can reach >50 dB and >30 dB for TE and TM polarizations, respectively, for some wavelength bands. The difference between the simulation results and the experimental results attribute to the fabrication imperfection.

A comparison of the PBS performances is given in Table 2 in the SOI platform. Generally, our proposed AM-based PBS performs low insert loss, high PER and small footprint, simultaneously. Though, the performance of Ref. [37] is better than our design. Our structures can reach > 40 dB and 30 dB PER for TE and TM polarizations, respectively, at certain wavelengths. In the other hand, Ref. [37] using the SU8 cladding to demonstrate the PBS, which is difficult to compatible with the device with Air cladding.

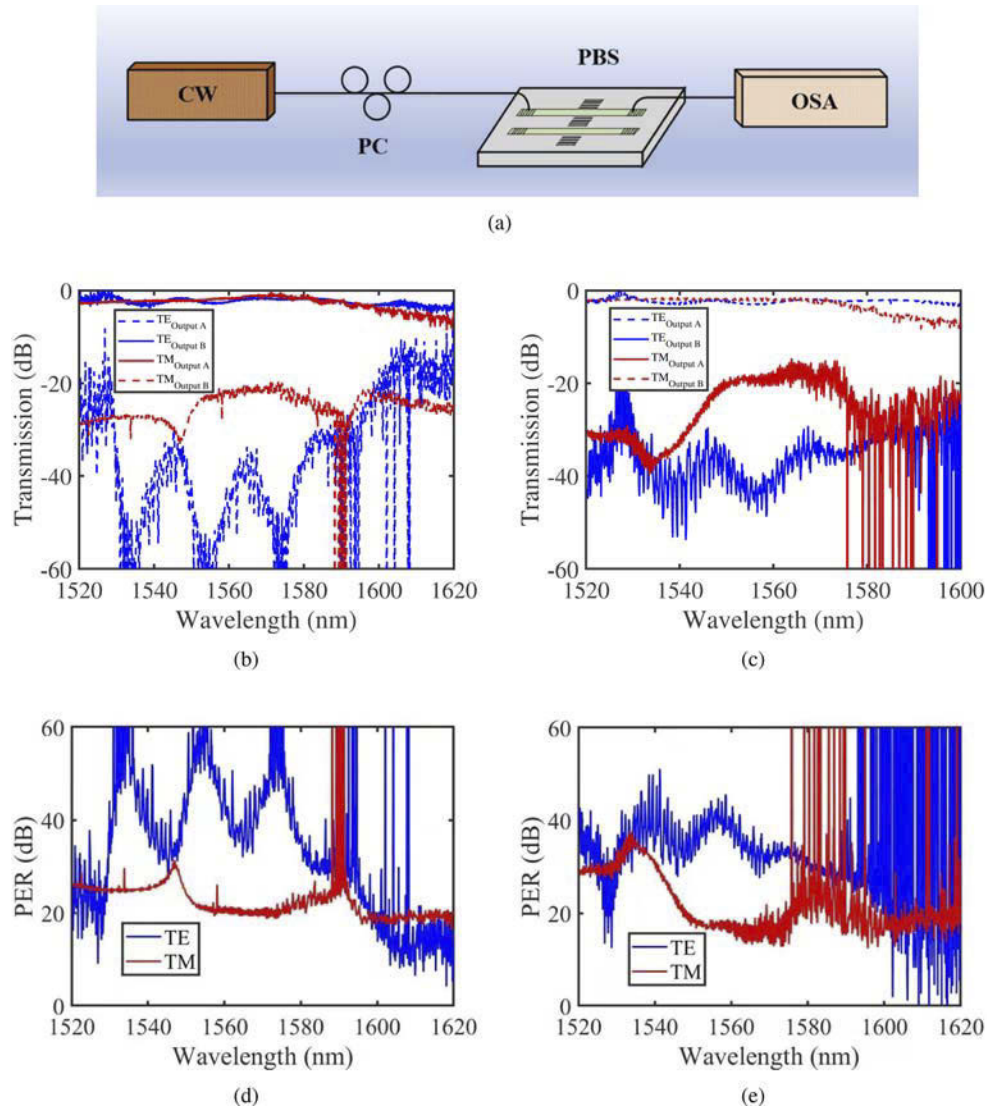


Fig. 6. (a) Measurement setup schematic. CW: continuous-waves laser source, PC: polarization controller, OSA: optical spectrum analyzer; The measured results of (b) transmission efficiency and (d) polarization extinction ratio as a function of wavelength with light input from Input A. The measured results of (c) transmission efficiency and (e) polarization extinction ratio as a function of wavelength with light input from Input B.

Table 2. Comparison of various AM-based PBS . FP: footprint, IL: insertion loss, PER: polarization extinction ratio, BW: bandwidth.

Work	FP (μm^2)	IL (dB)	PER (dB)	BW (nm)
Reference [38]	2.5×92.7	2.5	11.7	84
Ref. [37]	1.9×12.25	1	20	200
Ref. [36]	4×92.4	1	13	120
Ref. [39]	1.3×4.6	0.5	10	160
This work	2.5×14	1	20	80

4. Discussion

As the coupling region of the proposed PBS is symmetric, so we think the transmittance and the PER with incident light from Input A or Input B should be the same. We measure the transmission and the PER, when the light is incident from Input B, which is shown Fig. 6(c) and Fig. 6(e). It shows that the transmission efficiency and the PER of both polarizations are different, compared to Fig. 6(b) and Fig. 6(d). The S-bend waveguide is a critical part for integrated photonic devices, which will also influence the performance of the PBS [42–44]. The difference is considered to be induced by the S-bend waveguides. As the two parallel coupling waveguides is very closed to each other, so two S-bend waveguides are used to separate them before and after the coupling region.

We also analyze the S-bend waveguide effect on the PBS performance by the FDTD simulation. The transmission and the PER with the incident light from Input B are plotted in Fig. 7.

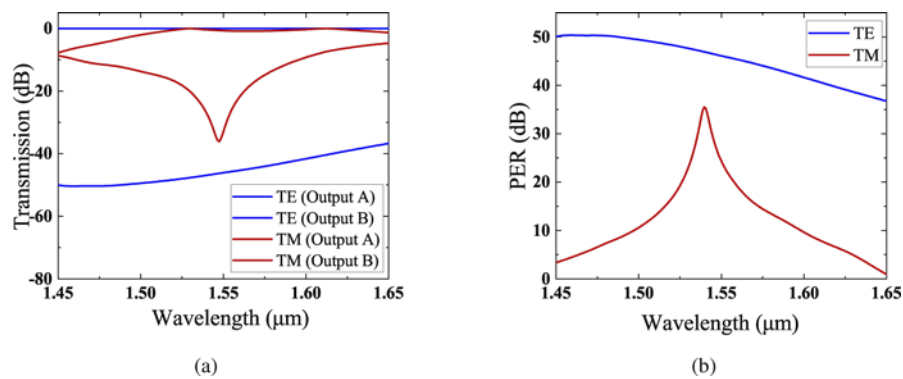


Fig. 7. (a) The transmission and (b) the PER versus wavelength.

Compared to Fig. 7 and Fig. 4(d), 4(e), the transmission and the PER with the light launched from Input A or Input B are different. The transmission efficiency is $> 90\%$ for both polarizations at the wavelength of 1.55 μm. The PER are 45dB and 35dB for TE and TM polarizations, respectively. According to the simulation results, the measured PER of the TE polarized light is a little higher, while that of the TM polarized light is a little lower, which is considered to be due to the coupling loss.

We then analyze how the vertical distance between the two straight waveguides of the S-bend waveguide affects the performance of the proposed AM PBS. We keep the horizontal length of the S-bend waveguide as 10 μm, and only change the vertical distance from 0.5 to 6.5 μm. Fig. 8 shows the transmission and the the PER versus the vertical distance. It shows that the TM polarization is more sensitive to the S-bend waveguide than the TE polarization. At the distance of 3 μm, the TM polarization exhibits the highest PER. The electric field distribution of the PBS with light incident from Input B is shown in Fig. 7, with the vertical distance of the S-bend waveguide as 0.5 μm, 3 μm, and 6.5 μm. From the figure, when the vertical distance is 0.5 or 6.5, the TM polarized light could not be maximally coupled into the adjacent waveguide, with obvious residual power remained in the incident waveguide, while the TE polarized light can maximally transmit directly without coupling. It means too close or too far distance can result in lower PER. When the height is 3 μm, the TM polarized light can be coupled maximally into the adjacent waveguide. In this case, the PBS shows the high transmittance and high PER of $> 94\%$ and 40 dB for both polarizations, respectively.

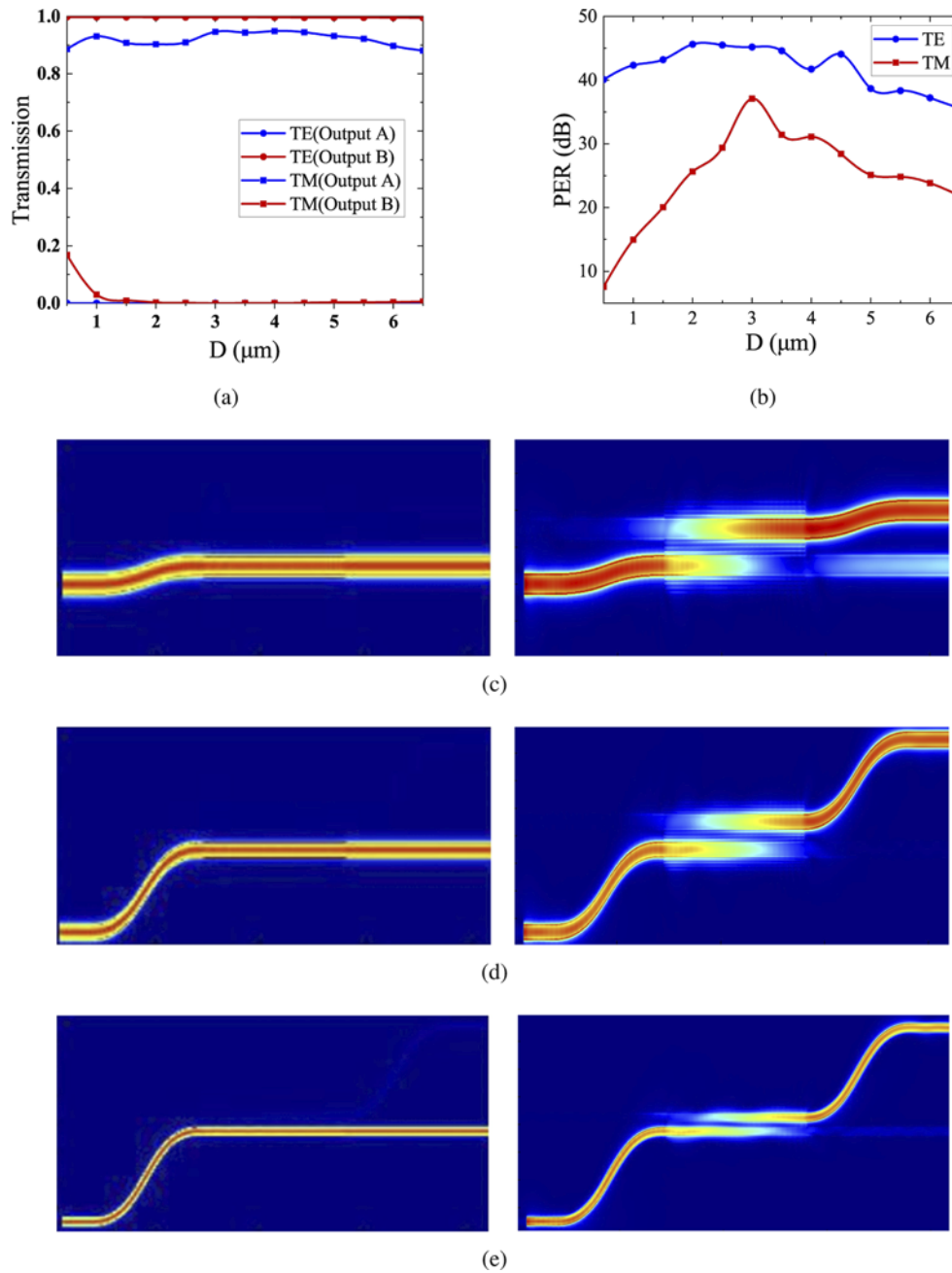


Fig. 8. (a) Simulated transmittance and (b) PER versus with the vertical distance of the S-bend waveguides, with incident light from Input B. Electric field distribution along the PBS with the vertical distance of the S-bend waveguides of (c) $0.5 \mu\text{m}$, (d) $3 \mu\text{m}$, and (e) $6.5 \mu\text{m}$.

5. Conclusion

In this paper, we have proposed an ultra-compact, low insertion loss, high PER polarization beam splitter, using the photonic anisotropic metamaterials. The device has a small footprint of

$2.5 \times 14 \mu\text{m}^2$. At the center wavelength of $1.55 \mu\text{m}$, the calculated insertion loss is less than 0.9 dB for both polarizations, and the polarization extinction ratio is higher than 40 dB and 30 dB for TE and TM polarizations, respectively. The experimental results shows that the insertion loss is < 1 dB for both polarizations, and the polarization extinction ratio is higher than 30 dB and 20 dB for TE and TM polarization, respectively, with a bandwidth of 80 nm. The result provide a way to design ultra-compact photonics device by using the anisotropic metamaterials.

Funding. China Postdoctoral Science Foundation (2019M651725); Natural Science Foundation of Jiangsu Province (BK20180862, BK20190839); Natural Science Research of Jiangsu Higher Education Institutions of China (20KJB140007); Program for New Century Excellent Talents in University (NCET-12-0142); Natural Science Foundation of Hunan Province (13JJ3001); Foundation of NUDT (JC13-02-13, ZK17-03-01); National Natural Science Foundation of China (60907003, 61805278, 62005074, 62005107).

Disclosures. The authors declare no conflicts of interest.

Data availability. The data that support the findings of this study are available from the corresponding author upon reasonable request.

References

1. Y. He, Y. Zhang, R. Zhang, L. Sun, and Y. Su, "Ultra-compact and broadband silicon polarizer employing a nanohole array structure," *Opt. Lett.* **46**(2), 194–197 (2021).
2. M. J. R. Heck, J. F. Bauters, M. L. Davenport, J. K. Doylend, S. Jain, G. Kurczveil, S. Srinivasan, Y. Tang, and J. E. Bowers, "Hybrid silicon photonic integrated circuit technology," *IEEE J. Sel. Top. Quantum Electron.* **19**(4), 6100117 (2013).
3. X. Shi, W. Fan, Y. Lu, A. K. Hansen, M. Chi, A. Yi, X. Ou, K. Rottwitt, and H. Ou, "Polarization and spatial mode dependent four-wave mixing in a 4h-silicon carbide microring resonator," *APL Photonics* **6**(7), 076106 (2021).
4. X. Shi, W. Fan, A. K. Hansen, M. Chi, A. Yi, X. Ou, K. Rottwitt, and H. Ou, "Thermal behaviors and optical parametric oscillation in 4h-silicon carbide integrated platforms," *Adv Photo Res* **2**(10), 2100068 (2021).
5. A. Billat, D. Grassani, M. Pfeiffer, S. Kharitonov, T. J. Kippenberg, and C.-S. Brès, "Large second harmonic generation enhancement in sin waveguides by all-optically induced quasi phase matching," *Nat. Commun.* **8**(1), 1016 (2017).
6. T. Findakly, P. Suchoski, and F. Leonberger, "High-quality litao3 integrated-optical waveguides and devices fabricated by the annealed-proton-exchange technique," *Opt. Lett.* **13**(9), 797–798 (1988).
7. J.-J. He, B. Lamontagne, A. ge, L. Erickson, M. Davies, and E. S. Koteles, "Monolithic integrated wavelength demultiplexer based on a waveguide rowland circle grating in ingaasp/inp," *J. Lightwave Technol.* **16**(4), 631–638 (1998).
8. P. Mataloni, "Integrated photonic quantum gates for polarization qubits," *Nat. Commun.* **2**, 1–6 (2011).
9. J. Zeuner, A. N. Sharma, M. Tillmann, R. Heilmann, M. Gräfe, A. Moqanaki, A. Szameit, and P. Walther, "Integrated-optics heralded controlled-not gate for polarization-encoded qubits," *npj Quantum Inf* **4**(1), 13 (2018).
10. L. Lu, L. Xia, Z. Chen, L. Chen, and X. S. Ma, "Three-dimensional entanglement on a silicon chip," *npj Quantum Inf* **6**(1), 30 (2020).
11. X. Qiang, X. Zhou, J. Wang, C. M. Wilkes, L. Thomas, O. Sean, K. Laurent, G. D. Marshall, S. Raffaele, and T. C. Ralph, "Large-scale silicon quantum photonics implementing arbitrary two-qubit processing," *Nat. Photonics* **12**(9), 534–539 (2018).
12. T. K. Liang and H. K. Tsang, "Integrated polarization beam splitter in high index contrast silicon-on-insulator waveguides," *IEEE Photonics Technol. Lett.* **17**(2), 393–395 (2005).
13. D. Dai, W. Zhi, N. Julian, and J. E. Bowers, "Compact broadband polarizer based on shallowly-etched silicon-on-insulator ridge optical waveguides," *Opt. Express* **18**(26), 27404–27415 (2010).
14. K. Tan, Y. Huang, G. Q. Lo, C. Yu, and C. Lee, "Experimental realization of an o-band compact polarization splitter and rotator," *Opt. Express* **25**(4), 3234–3241 (2017).
15. W. Hao, T. Ying, and D. Dai, "Ultra-broadband high-performance polarizing beam splitter on silicon," *Opt. Express* **25**(6), 6069–6075 (2017).
16. Y. Ding, L. Liu, C. Peucheret, and H. Ou, "Fabrication tolerant polarization splitter and rotator based on a tapered directional coupler," *Opt. Express* **20**(18), 20021–20027 (2012).
17. Z. Cheng, J. Wang, Y. Huang, and X. Ren, "Realization of a compact broadband polarization beam splitter using the three-waveguide coupler," *IEEE Photonics Technol. Lett.* **31**(22), 1807–1810 (2019).
18. X. Guan, H. Wu, Y. Shi, and D. Dai, "Extremely small polarization beam splitter based on a multimode interference coupler with a silicon hybrid plasmonic waveguide," *Opt. Lett.* **39**(2), 259 (2014).
19. M. Aamer, A. M. Gutierrez, A. Brimont, D. Vermeulen, G. Roelkens, J. M. Fedeli, A. Hakansson, and P. Sanchis, "Cmos compatible silicon-on-insulator polarization rotator based on symmetry breaking of the waveguide cross section," *IEEE Photonics Technol. Lett.* **24**(22), 2031–2034 (2012).
20. D. Dai, Z. Wang, J. Peters, and J. E. Bowers, "Compact polarization beam splitter using an asymmetrical mach-zehnder interferometer based on silicon-on-insulator waveguides," *IEEE Photonics Technol. Lett.* **24**(8), 673–675 (2012).

21. D. Dai and J. E. Bowers, "Novel ultra-short and ultra-broadband polarization beam splitter based on a bent directional coupler," *Opt. Express* **19**(19), 18614–18620 (2011).
22. B. Bai, L. Liu, and Z. Zhou, "Ultracompact, high extinction ratio polarization beam splitter-rotator based on hybrid plasmonic-dielectric directional coupling," *Opt. Lett.* **42**(22), 4752–4755 (2017).
23. K. W. Chang and C. C. Huang, "Ultrashort broadband polarization beam splitter based on a combined hybrid plasmonic waveguide," *Sci. Rep.* **6**(1), 19609 (2016).
24. J. Huang, J. Yang, D. Chen, X. He, Y. Han, J. Zhang, and Z. Zhang, "Ultra-compact broadband polarization beam splitter with strong expansibility," *Photon. Res.* **6**(6), 574–578 (2018).
25. L. H. Gabrielli, D. Liu, S. G. Johnson, and M. Lipson, "On-chip transformation optics for multimode waveguide bends," *Nat. Commun.* **3**(1), 1217 (2012).
26. J. Huang, J. Yang, D. Chen, W. Bai, J. Han, Z. Zhang, J. Zhang, X. He, Y. Han, and L. Liang, "Implementation of on-chip multi-channel focusing wavelength demultiplexer with regularized digital metamaterials," *Nanophotonics* **9**(1), 159–166 (2019).
27. Bing Shen, Peng Wang, Randy Polson, and Rajesh Menon, "An integrated-nanophotonics polarization beamsplitter with $2.4 \times 2.4 \mu\text{m}^2$ footprint," *Nat. Photonics* **9**(6), 378–382 (2015).
28. X. Guan, P. Chen, S. Chen, P. Xu, Y. Shi, and D. Dai, "Low-loss ultracompact transverse-magnetic-pass polarizer with a silicon subwavelength grating waveguide," *Opt. Lett.* **39**(15), 4514–4517 (2014).
29. S. Jahani and Z. Jacob, "All-dielectric metamaterials," *Nat. Nanotechnol.* **11**(1), 23–36 (2016).
30. L. H. Gabrielli, J. Cardenas, C. B. Poitras, and M. Lipson, "Silicon nanostructure cloak operating at optical frequencies," *Nat. Photonics* **3**(8), 461–463 (2009).
31. M. G. Silveirinha, A. Alù, and N. Engheta, "Parallel-plate metamaterials for cloaking structures," *Phys. Rev. E* **75**(3), 036603 (2007).
32. J. Zhang, J. Yang, X. He, H. Jie, and Z. Zhang, "Ultrashort and efficient adiabatic waveguide taper based on thin flat focusing lenses," *Opt. Express* **25**(17), 19894–19903 (2017).
33. J. Hunt, T. Tyler, S. Dhar, Y.-J. Tsai, P. Bowen, S. Larouche, N. M. Jokerst, and D. R. Smith, "Planar, flattened lüneburg lens at infrared wavelengths," *Opt. Express* **20**(2), 1706–1713 (2012).
34. T. Paul, C. Rockstuhl, C. Menzel, and F. Lederer, "Anomalous refraction, diffraction, and imaging in metamaterials," *Phys. Rev. B* **79**(11), 115430 (2009).
35. M. Y. Shalaginov, S. An, Y. Zhang, F. Yang, and T. Gu, "Reconfigurable all-dielectric metalens with diffraction-limited performance," *Nat. Commun.* **12**(1), 1225 (2021).
36. A. Herrero-Bermello, A. Dias-Ponte, J. M. Luque-González, A. O.-M. nux, A. V. Velasco, P. Cheben, and R. Halir, "Experimental demonstration of metamaterial anisotropy engineering for broadband on-chip polarization beam splitting," *Opt. Express* **28**(11), 16385–16393 (2020).
37. H. Xu, D. Dai, and Y. Shi, "Ultra-broadband and ultra-compact on-chip silicon polarization beam splitter by using hetero-anisotropic metamaterials," *Laser & Photonics Reviews* **13**, 18003491 (2019).
38. L. Xu, Y. Wang, A. Kumar, D. Patel, E. El-Fiky, Z. Xing, R. Li, and D. V. Plant, "Polarization beam splitter based on mmi coupler with swg birefringence engineering on soi," *IEEE Photonics Technol. Lett.* **30**(4), 403–406 (2018).
39. S. Mao, L. Cheng, C. Zhao, and H. Y. Fu, "Ultra-broadband and ultra-compact polarization beam splitter based on a tapered subwavelength-grating waveguide and slot waveguide," *Opt. Express* **29**(18), 28066–28077 (2021).
40. M. B. Mia, S. Z. Ahmed, I. Ahmed, Y. J. Lee, M. Qi, and S. Kim, "Exceptional coupling in photonic anisotropic metamaterials for extremely low waveguide crosstalk," *Optica* **7**(8), 881–887 (2020).
41. <https://www.lumerical.com/tcad-products/fdtd/>.
42. N. Zamhari and A. A. Ehsan, "Large cross-section rib silicon-on-insulator (soi) s-bend waveguide," *Optik* **130**, 1414–1420 (2017).
43. H. Yu, X. Sun, D. Ban, and F. Qiu, "Propagation of fundamental mode in regularly bending multi-mode waveguides," *Opt. Quantum Electron.* **53**(7), 408 (2021).
44. Y. Liu, K. Xu, S. Wang, W. Shen, H. Xie, Y. Wang, S. Xiao, Y. Yao, and D. J. Z. He, "Arbitrarily routed mode-division multiplexed photonic circuits for dense integration," *Nat. Commun.* **10**(1), 3263 (2019).